Corrosion Study of Super Ferritic Stainless Steel UNS S44660 (26Cr-3Ni-3Mo) and Several Other Stainless Steel Grades (UNS S31603, S32101, and S32205) in Caustic Solution Containing Sodium Sulfide

KEVIN R. CHASSE and PREET M. SINGH

Electrochemical techniques, scanning electron microscopy (SEM), and X-ray photoelectron spectroscopy (XPS) were used in this study to show how the corrosion mechanism of several commercial grades of stainless steel in hot caustic solution is strongly influenced by the presence of sodium sulfide. Experimental results from super ferritic stainless steel UNS S44660 (26Cr-3Ni-3Mo) were compared to austenitic stainless steel UNS S31603, lean duplex stainless steel (DSS) UNS S32101, and standard DSS UNS S32205 in caustic solution, with and without sodium sulfide, at 443 K (170 °C). Weight loss measurements indicated that corrosion rates of UNS44660 were much lower than the other grades of stainless steel in the presence of the sodium sulfide. Potentiodynamic polarization and linear polarization resistance measurements showed that the electrochemical behavior was altered by the adhesion of sulfur species, which reduced the polarization resistances and increased the anodic current densities. SEM and XPS results imply that the surface films that formed in caustic solution containing sodium sulfide were defective due to the adsorption of sulfide, which destabilized the passive film and led to the formation of insoluble metal sulfide compounds.

DOI: 10.1007/s11661-013-1878-5

I. INTRODUCTION

THE corrosion resistance of stainless steel depends on the oxide film that forms on the surface, which is a function of the alloy composition, microstructure, and the environment. Super ferritic stainless steels (SFSS) generally have superior corrosion resistance to their austenitic counterparts because of their higher Cr contents and ferritic microstructures; however, the use of SFSS has been somewhat limited by poor weldability and low toughness in certain applications.[1–3] SFSS are less tolerant to secondary phases and have a low solubility of interstitial elements such as C and N. Ti and Cb additions are also required to control the detrimental effects of interstitial elements. Most SFSS in service today are used in thin-walled tubing or tube sheet sections in seawater and high-chloride environments, such as power plant condensers, multistage desalination plants, and numerous heat exchanger applications. Since the mid-1970s, modified grades of super ferritic as well as austenitic-ferritic, duplex stainless steels (DSSs) have been developed for certain chemical process environments where the strength and/or corrosion resistance of 300 series austenitic grades, *i.e.*, AISI 316 and AISI 304, are inadequate for service. Processes using caustic soda (NaOH), *i.e.*, sodium hydroxide, such as the kraft process in pulp and paper manufacture, petrochemical refining to remove hydrogen sulfide (H_2S) gas and mercaptans from sour hydrocarbon streams, the girdler sulfide process in heavy water treatment, and alumina extraction in the Bayer process, are such service environments. Laboratory and field experience[4–18] have demonstrated that the 300 series austenitic stainless steels and the austenitic phase of lean and standard DSS are susceptible to selective corrosion and stress corrosion cracking (SCC) at elevated temperatures in caustic service, particularly when sodium sulfide (Na_2S) is present.

The corrosion of stainless steel in kraft pulping liquors has been the subject of a number of investigations. Nichol *et al.*[1] showed that SFSS grade XM-27 was considerably more corrosion resistant than austenitic grades in extracted white and black liquors at 443 K (170 °C) based on weight loss studies. Wensley *et al.*[5,6] performed weight loss measurements in conjunction with potentiostatic polarization on select austenitic, DSSs, and stainless steel weld overlays in extracted white and black (3:1) liquors at 443 K (170 °C) and showed that increasing the Cr content above 25 wt pct was necessary for enhanced corrosion resistance. The austenitic phase was attacked preferentially in the DSSs at potentials more noble than the open circuit potential (OCP). The distribution of phases and partitioning of alloying elements in the two phases (*i.e.*, Cr, Ni, and Mo) are an important parameter controlling the corrosion properties of DSSs. Bhattacharya and Singh[9] studied the electrochemical behavior

KEVIN R. CHASSE, Ph.D. Candidate and PREET M. SINGH, Professor, are with the School of Materials Science and Engineering, Georgia Institute of Technology, 771 Ferst Drive, N.W., Atlanta, GA 30332-0245. Contact e-mail: kevin.chasse@gmail.com
Manuscript submitted May 28, 2012.
Article published online July 23, 2013

and film structure of different DSSs and their alloying elements in simulated white liquor using potentiodynamic polarization and X-ray diffraction (XRD) and showed that alloying Fe with Cr and Ni shifted the OCP in the electropositive direction and reduced the critical current density of the DSSs. The passive films formed under these conditions consisted primarily of spinel oxides of Fe, Ni, and Cr. Ramo *et al.*[19,20] studied the interaction of sulfur anions with various stainless grades (UNS S30400, S31603, S32205, and S32304) using X-ray fluorescence (XRF) and contact electrical resistance (CER) in simulated white liquors. Their work showed that hydroxide content was found to correlate linearly with the adhesion of sulfur onto steel, whereby hydroxide enhanced the sulfur rich film formation on stainless steel surfaces. Adhesion of sulfur onto surfaces increased in the order: UNS S32304, S32205, S30400, and S31603. Betova *et al.*[21] used electrochemical impedance spectroscopy to study UNS S31603 and its constituents in simulated white liquor at 443 K (170 °C) and showed that sulfide adsorption leads to significant change in the corrosion kinetics from a process controlled by solid-state transport to an interfacial-controlled process similar to active dissolution.

The composition and structure of the oxide film formed on the surface of stainless steel has been the subject of many investigations.[22] Corrosion resistance of stainless steel is attributed to Cr enrichment of the passive film in the form of a bi-layer oxyhydroxide mixture. The film is thinner and less defective with increasing Cr content.[23–29] The Cr content in the passive film is a strong function of the alloy composition, solution, temperature, and electrode potential. Most studies on the passivation of stainless steels in sulfide-containing solution have been conducted at ambient temperatures with respect to soil environments or polluted marine environments containing sulfate-reducing bacteria (SRB).[30–34] The transformation of the metal oxides to metal sulfides is influenced by the interaction with the bacteria in these low-temperature environments; however, the mechanism by which sulfide adsorption influences the composition and structure of the surface of stainless steels in hot caustic solution is not well understood, particularly in kraft pulping environments containing white liquor.

The primary objective of the current study was to assess the effect of sodium sulfide on the corrosion mechanism of a 26Cr-3Ni-3Mo, SFSS UNS S44660 in hot caustic solution simulating white liquor and compare the results to austenitic UNS S31603, lean DSS UNS S32101, and standard DSS UNS S32205. The corrosion behavior near the OCP was evaluated by weight loss measurements and electrochemical techniques, *i.e.*, potentiodynamic polarization and linear polarization resistance (LPR). The film morphologies were observed with scanning electron microscopy (SEM) equipped with an energy dispersive X-ray spectroscopy (EDS) detector following exposure. Composition of the films were determined as a function of depth with X-ray photoelectron spectroscopy (XPS) equipped with sputtering capability to understand the relationship between material composition and the influence of sulfide on the oxide films in 2.5 M NaOH, with and without 0.70 M Na_2S, at 443 K (170 °C).

II. EXPERIMENTAL PROCEDURES

A. *Specimens and Test Solutions*

The SFSS was provided as 1.000'' outer diameter × 0.065'' nominal wall thickness welded tubing per ASTM A268.[34] The austenitic stainless steel, lean DSS, and standard DSS were provided as 0.625'' nominally thick plate in the as-received, mill condition per ASTM A240.[35] The nominal chemical compositions (wt pct) of the SFSS (UNS S44660), austenitic (UNS S31603), lean DSS (UNS S32101), and standard DSS (UNS S32205) materials used in this study are listed in Table I.

Experiments were conducted using 100 g/L NaOH (2.5 M) and 100 g/L NaOH + 55 g/L Na_2S (0.70 M) solutions at 443 K (170 °C). The solutions were prepared by dissolving 100 g of NaOH and 100 g of NaOH + 169.7 g of $Na_2S{\cdot}9H_2O$ into 1000 mL of deionized water, respectively. The samples were exposed to the environments for 168 hours at the OCP. Preliminary studies showed that OCP remained stable (within ±1 mV for 10 minutes) after approximately 72 hours of exposure.

B. *Weight Loss Measurements*

All experiments were carried out at 443 K ± 1 K (170 °C ± 1 °C) for 168 hours in a 2-liter autoclave with an external temperature control through a K-type thermocouple held in a thermowell in the autoclave lid. It took approximately 2 hours to reach the test temperature. Samples were placed on a polytetrafluoroethylene (PTFE)—insulated rod and electrically isolated with PTFE washers. Duplicate samples were used to insure minimal sample-to-sample variation, which was found to be ±10 pct for all materials. Reported values are the average of two measurements.

Prior to each experiment, samples were weighed with a precise scale with an accuracy of ±0.0001 g. The dimensions were measured with a dial caliper having an accuracy of ±0.01 mm. The average corrosion rate was calculated from the weight change during test. Upon completion of each weight loss test, samples were rinsed in distilled water. The samples were then placed in an airlock bag and placed in an evacuated chamber that contained desiccant to preserve the sample surface condition. Films were removed on select samples with an inhibited acid solution (Clark's solution) having a concentration of 50 g $SnCl_2$ + 20 g/L Sb_2O_3 in 1000 mL HCl prior to weight loss measurements. Blank samples were also exposed to the Clark's solution and weighed to insure no metal loss from the cleaning process alone.

The sample surfaces were examined with standard microscopy techniques following the weight loss tests to detect the form of corrosion and surface morphology. Optical microscopy was used to characterize the surface at low magnifications (<500 times magnification), and SEM was used to study the surface morphology at

Table I. Nominal Chemical Composition (Weight Percent) of the Materials Used in this Study

UNS Number	Grade/Type	C (Max)	Mn (Max)	P (Max)	S (Max)	Si (Max)	Cr	Ni	Mo	N (Max)	Cu (Max)	Other
S44660	26-3-3	0.030	1.00	0.040	0.030	1.00	25.0 to 28.0	1.0 to 3.50	3.0 to 4.0	0.040	—	*
S31603	316L	0.030	2.00	0.045	0.030	0.75	16.0 to 18.0	10.0 to 14.0	2.00 to 3.00	0.10	—	—
S32101	LDX 2101®**	0.040	4.00 to 6.00	0.040	0.030	1.00	21.0 to 22.0	1.35 to 1.70	0.10 to 0.80	0.20 to 0.25	0.10 to 0.80	—
S32205	2205	0.030	2.00	0.030	0.020	1.00	22.0 to 23.0	4.5 to 6.5	3.0 to 3.5	0.14 to 0.20	—	—

*(Ti + Cb) = 0.20–1.00 and 6 × (C + N) min.
**LDX 2101® is a registered trademark of Outokumpu Stainless, Espoo, Finland.

higher magnifications. The surfaces were analyzed with accelerating energy of 15 kV using the secondary electron detector. EDS was used to evaluate the composition of the corrosion films in several cases.

C. *Electrochemical Measurements*

All experiments were carried out at 443 K ± 1 K (170 °C ± 1 °C) over a 168 hours period using a Gamry Reference 600* potentiostat–galvanostat. The surfaces of the specimens were mechanically wet polished with 600 grit SiC paper, rinsed with deionized water, and degreased with acetone before each test. The exposed surface area of the specimens was approximately 5 cm^2. The experiments were conducted using a conventional three-electrode setup. Electrodes machined from plate were threaded onto a PTFE—insulated leads and electrically isolated from the autoclave. A platinum foil was used as the counter electrode, and a Mo/MoS_2 rod was used as the pseudo reference electrode. The potential of the reference electrode was approximately −1050 ± 25 mV *vs* Ag/AgCl at the test temperature. The electrochemical setup that was used in the autoclave is shown in Figure 1.

The OCP was allowed to stabilize for 24 hours prior to running each potentiodynamic scan. During the potentiodynamic scans, the potential was increased in the electropositive direction at a sweep rate of 2 mV s^{-1} beginning −0.3 V *vs* the OCP while the current was measured. The scans were stopped when the peak current reached 0.5 A, which was the upper limit of the potentiostat–galvanostat. Quasi-steady-state current *vs* potential curves were measured. Experiments were repeated in several cases to insure reliability of the results. Samples were removed from the autoclave after each experiment and further characterized.

Linear polarization resistance (LPR) was measured in a separate experiment over a 168 hours period every 24 hours at a sweep rate of 0.01 mV s^{-1} beginning −10 mV *vs* the OCP and ending +10 mV *vs* the OCP. Measurements of the OCP were made prior to each scan. The corrosion rate, r, and polarization resistance, R_p, values were determined by curve fitting with electrochemical analysis (Gamry's Echem Analyst**) software based on

$$r = \frac{ia}{nF} \quad [1]$$

$$i = \frac{\beta_a \beta_c}{2.303 R_p (\beta_a + \beta_c)} \quad [2]$$

*Reference 600™ is a trademark of Gamry Instruments, Philadelphia, PA.

**Echem Analyst™ is a trademark of Gamry Instruments, Philadelphia, PA.

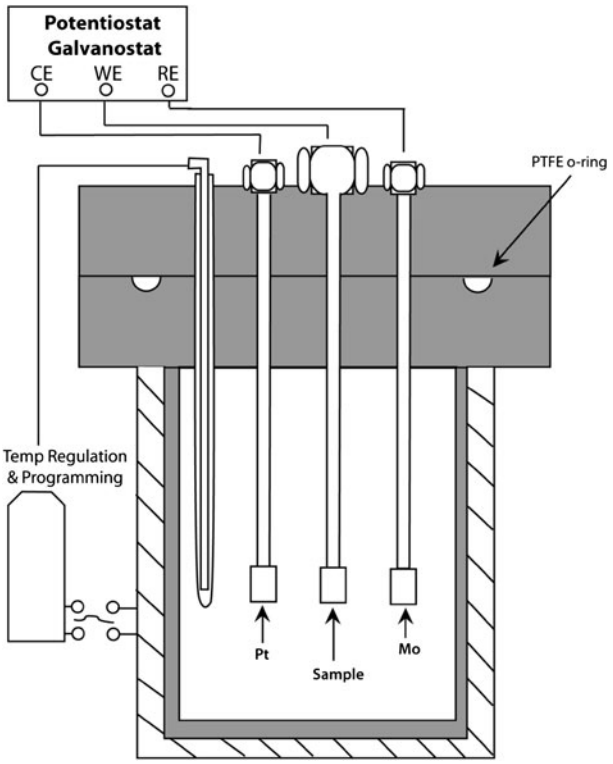

Fig. 1—Schematic of the experimental configuration used for the electrochemical measurements.

where i, the current density, equals I/A, the current divided by the surface area. The atomic weight, a, and number of electrons n depend on the particular element and are expressed as the equivalent weight. F is Faraday's constant. The Tafel constants, β_a and β_c were extrapolated from the potentiodynamic scans using a logarithmic fit. R_p is taken as the linear slope of the line over the 20 mV range.

D. *Scanning Electron Microscopy*

Samples were mounted in a conductive phenolic resin and cross-sectioned with a diamond blade saw. The mounts were ground to 1000 grit silicon carbide paper using lapping oil as a lubricant to preserve the oxide film. A final polish of 0.25 μm was performed with a diamond paste suspension. The samples were rinsed with acetone and dried under hot air. The cross-sectioned samples were observed in a SEM equipped with an EDS detector. An accelerating voltage of 15 kV was used to measure the composition of the oxide films formed on the surface of samples exposed to the test solution. A minimum of 15 points was sampled in different regions of the sample film. The magnification depended on the film thickness.

E. *X-ray Photoelectron Spectroscopy*

A section of each tested sample was stored in a desiccator until analysis could be performed. Surface analysis of the films was made under ultra high vacuum with an X-ray spectrometer equipped with an argon ion gun for sputtering capability. An aluminum anode (1486.7 eV) was used to generate photoelectrons. A flood gun was used to maintain charge neutrality on the surface. Photoelectrons were collected over an analysis region of 1.25 mm^2 with the surface orientated normal to the analyzer entrance. A survey scan in the energy range 0 to 1100 eV with pass energy of 50 eV was first acquired to detect elements on the surface layer. The C 1s peak (284.6 eV) was used to check the energy scale. High-resolution scans were performed with pass energy of 20 eV on the primary alloying elements and solution constituents. Sputtering was performed with energy of 3 kV over a 2 mm raster size. The depth was calculated based on a tantalum oxide (Ta_2O_5) reference. Data analysis was performed with commercial fitting software (Thermo Fisher Scientific Avantage[†]) using Shirley background subtraction and Lorentzian–Gaussian peak fitting to determine the composition and chemical states at the oxide/metal interface taken as approximately one half of the maximum O 1s peak intensity.

[†]Avantage Data System is a product of Thermo Fisher Scientific Inc., Waltham, MA.

III. RESULTS AND DISCUSSION

A. *Corrosion Rates*

Figure 2 shows the corrosion rates based on weight loss for the stainless alloys tested in the 2.5 NaOH caustic solutions, with and without 0.70 M Na_2S, at 443 K (170 °C) for 168 hours. Pitting was not observed in either of the test solutions, thus the reported rates for all of the stainless steels are for general corrosion. Selective corrosion of austenite was observed in the DSSs tested in the sulfide-containing solution, but the selective attack was generally limited. The SFSS UNS S44660 had a corrosion rate of nearly 0.1 mm/year in the simple NaOH solution. The addition of Na_2S did not appear to result in an increase in the corrosion rate of the SFSS. Conversely, an appreciable increase in the corrosion rates was found for austenitic and DSSs tested in 2.5 M NaOH + 0.70 M Na_2S as compared to the simple NaOH solution. Austenitic UNS S31603 had the lowest corrosion rate (0.02 mm/year) in the simple NaOH solution and had the highest corrosion rate (0.31 mm/year) in the sulfide-containing solution. SFSS UNS S44660 had the lowest corrosion rate (0.05 mm/year) of the stainless steels that were tested with the addition of sulfide. The corrosion rates of the lean DSS (0.26 mm/year) and standard DSS (0.25 mm/year) in the sulfide-containing solution were lower than the austenitic stainless steel and higher than the SFSS. The results in Figure 2 support earlier findings that showed higher Cr, which is beneficial for corrosion resistance in sulfide-containing, caustic solution. Wensley *et al.*[5,6] showed that increasing the Cr content above 25 wt pct was necessary for enhanced corrosion resistance in alkaline

pulping liquors. Cr provides a protective film of chromium hydroxide or oxide on stainless steels in alkaline environments.[22]

B. *Potentiodynamic Polarization*

Table II summarizes the potentiodynamic polarization results where corrosion rates were determined by the Tafel extraction technique. Corrosion rates of the stainless steels were generally less than 0.10 mm/year in the simple NaOH environment (C). The results from a Pt foil tested in the two solutions are shown for comparison. Results of Pt foil tested in sulfide-containing solution (SC) indicated that the oxidation/reduction of sulfur species likely accounted for much of the increase in the observed anodic current densities and change in Tafel slope behavior. Therefore, the interpretation of the potentiodynamic results and corresponding corrosion rates are obfuscated in the sulfide-containing solution due to the oxidation/reduction of sulfur species and corresponded to the S^{2-}/SO_4^{2-} equilibrium reaction.[9] The trends in the measured corrosion rates were analogous to the weight loss measurements with the addition of sulfide. The addition of sulfide resulted in an increase in the corrosion rates for all of the alloys with the lowest rate being observed for the SFSS UNS S44660. The highest rate was found for austenitic UNS S31603 with intermediate rates for the duplex grades UNS S32101 and UNS S32205. The current densities were greater in the presence of sulfide. The lean DSS UNS S32101 did not show a large increase in critical current density, i_{CORR}, as compared to the other alloys. Results also show that there was an appreciable reduction in the anodic Tafel slopes of the stainless alloys tested in the sulfide-containing solution, particularly for the SFSS. The OCP became more electronegative for the SFSS UNS S44660 as well as the austenitic grade S31603, whereas this value became more electropositive for lean DSS UNS S32101 and standard DSS UNS S32205.

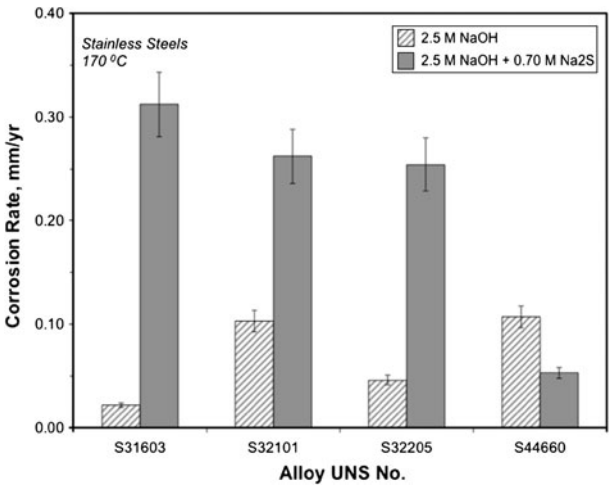

Fig. 2—Corrosion rates (mm/year) of SFSS UNS S44660, austenitic UNS S31603, lean DSS UNS S32101, and standard DSS S32205 tested in 2.5 M NaOH as well as 2.5 M NaOH + 0.70 M Na_2S at 443 K (170 °C).

The anodic polarization curve of SFSS UNS S44660 tested in 2.5 M NaOH at 443 K (170 °C) is compared to austenitic UNS S31603, lean DSS UNS S32101, standard DSS UNS S32205, and Pt foil in Figure 3. The OCP or E_{OC} of the SFSS was more electropositive than the other stainless steel alloys in the simple NaOH solution. Moreover, there was a higher current density at anodic potentials that was likely associated with the transpassive dissolution of Cr based on earlier electrochemical studies of stainless steel.[8,9] The general shapes of the polarization curves were similar for the stainless steels. The Tafel slopes were approximately linear at potentials just negative to the OCP, indicating that there was a charge-transfer process.[21] The cathodic current density was nearly an order of magnitude greater for UNS S31603, indicating that there was an increase in this charge-transfer process. The anodic activity was enhanced in UNS S32205 and UNS S31603 as compared to UNS S32101 and S44660. The cathodic Tafel slopes are similar in the caustic environments, which supports a cathodic reaction due to hydrogen evolution.

Other electrochemical studies[8,9,21] have used thermodynamic predictions to determine the principal reactions for different grades of stainless steels and their primary alloying elements (Fe, Cr, Ni, and Mo) in simple NaOH environments. A recent study by Betova *et al.*[21] evaluated the anodic polarization behavior of

Table II. Anodic Polarization Parameters of Select Materials Tested in 2.5 M NaOH (C) and 2.5 M NaOH + 0.70 M Na_2S (SC) at 443 K (170 °C) Determined from Tafel Extraction

Alloy UNS Number	Env.	icorr (μA cm^{-2})	E_{OC} (mV *vs* MoS_2)	βa (mV dec^{-1})	βc (mV dec^{-1})	Corrosion rate (mm year^{-1})*
S44660	C	80	140	613	1000000	0.094
S44660	SC	423	7	66	283	0.801
S31603	C	131	102	318	1000000	0.154
S31603	SC	226	59	81	1000000	5.53
S32101	C	158	−139	206	104	0.047
S32101	SC	190	71	54	208	1.24
S32205	C	151	−8	315	116	0.044
S32205	SC	439	18	53	216	2.92
Pt	C	28	518	160	242	0.020
Pt	SC	125	−28	83	190	6.54

*Corrosion rates listed here were calculated assuming that the metal oxidation is the only anodic reaction.

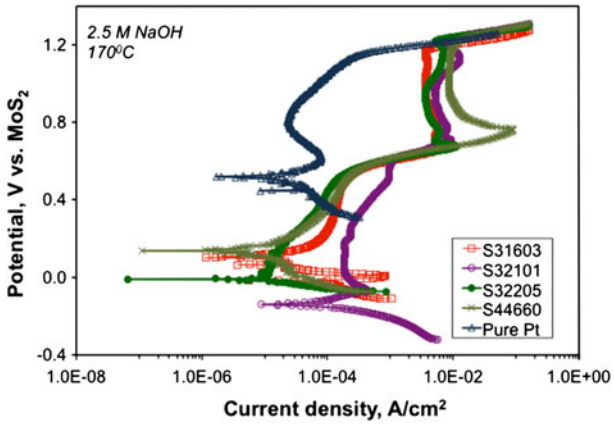

Fig. 3—Anodic polarization curves of SFSS UNS S44660, austenitic UNS S31603, lean DSS UNS S32101, standard DSS UNS S32205, and pure Pt tested in 2.5 M NaOH at 443 K (170 °C).

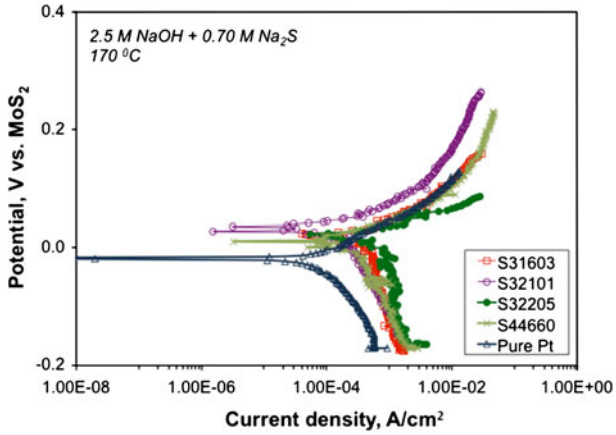

Fig. 4—Anodic polarization curves of SFSS UNS S44660, austenitic UNS S31603, lean DSS UNS S32101, and standard DSS UNS S32205, and pure Pt tested in 2.5 M NaOH + 0.70 M Na_2S at 443 K (170 °C).

AISI 316L stainless steel and its primary alloying elements in 2.5 M NaOH at 443 K (170 °C) to determine compositional effects on the electrochemical behavior. Studies in simple NaOH solutions demonstrated that increased Cr and Ni content in austenitic stainless steel reduced the critical current density required for passivation and shifted the OCP in the electropositive direction. The oxides of Cr and Ni are protective in alkaline environments. Cr is also beneficial in hot lithium hydroxide due to the formation of chromium hydroxide or oxide compounds.[8] The role of Mo and Ni are unclear from these data, but Mo has extensively been shown to be detrimental in alkaline solutions due to the formation of soluble molybdate MoO_4^{2-} or molybdate ions.[5,6,9] Mo has been shown to be beneficial to DSSs in other media depending on the concentration. Jang *et al.* studied the effect of Mo in cast CD4MCU DSSs in acidified chloride-containing media and showed that the addition of 2 wt pct Mo was detrimental to the corrosion properties due to an increase in the volume fraction of the ferritic phase.[36] With the addition of 4 wt pct Mo, however, the corrosion performance improved. The earlier electrochemical studies and thermodynamic predictions[8,9] have shown that Ni forms a stable film in simple caustic solution. The various electrochemical reactions that can occur on stainless steels in NaOH environments have been reported in detail and will not be discussed here further.

Addition of sulfide had a considerable influence on the potentiodynamic behavior of the alloys in the 2.5 M NaOH + 0.70 M Na_2S solution as shown in Figure 4. No clear differences can be observed in the polarization curves due to the influence of the oxidation/reduction of sulfur species at the electrode surface. Furthermore, it was not possible to determine the polarization behavior beyond 0.200 V electropositive to the OCP due to the current limitations of the potentiostat–galvanostat. Shoesmith *et al.*[37] attributed the large increase in anodic current density in the presence of sulfide to the reactive adsorption of sulfide on the surface of Fe, which hampers the growth of the passive film and increases its defective structure. Tromans[38] and Salvarezza *et al.*[39] applied different electrochemical techniques and found similar effects of sulfide on the surface film of carbon steel. The sulfide reacts with metallic cations in the outer layer and leads to the formation of sulfur-containing phases through the following reaction:

$$M_M^{2+} + HS_{ad}^- = MHS_{ad}^+ + V_M'' \qquad [3]$$

$$MHS_{ad}^+ = MS_{1-x} + xHS^- + (1-x)H^+. \qquad [4]$$

Electrochemical results from more recent studies on stainless steel[9,21] have led to similar conclusions on the role of sulfide based on thermodynamic predictions. The OCP of the alloys was near the region where nickel sulfide (Ni_3S_2) and iron sulfide (FeS) may form based on the E-pH diagram for the S-Fe-Cr-Ni–H_2O system at 443 K (170 °C).[40,41] The sulfur-enriched surface results in a higher defect concentration of the film, thus increasing its ionic conductivity of the oxide film formed on the alloy surface.[38,39] The formation of metal sulfides may also lead to local acidification and increased dissolution of the surface film. The individual contributions of the alloying elements were not measured in the current study because electrochemical studies[9,21] of Fe, Cr, Ni, and Mo have been performed under similar caustic conditions. Metal sulfide compounds may form on stainless steel near the OCP in sulfide-containing solution. Complex metal salts, such as sodium ferric sulfide ($NaFeS_2$), can also form in these environments based on XRD measurements.[9]

C. *LPR Measurements*

LPR measurements from the stainless steel samples exposed to 2.5 M NaOH and 2.5 M NaOH + 0.70 M Na_2S over at 168 hours period at 443 K (170 °C) are shown in Figures 5(a) and (b), respectively. The polarization resistance of the SFSS UNS S44660 in the simple NaOH solution was not appreciably different from the austenitic UNS S31603 or standard DSS UNS S32205 over the 168 hours test period. Results in the simple

NaOH solution indicate that the polarization resistance values continued to increase with exposure time indicating that the films were becoming more protective; however, no increase was observed in lean DSS S32101. Polarization resistance values varied from ~4 kΩ cm^2 for the lean DSS UNS S32101 to ~20 kΩ cm^2 for SFSS UNS S44660, austenitic UNS S31603, and standard DSS UNS S32205 after the 168 hours exposure. Previous attempts by Crowe and Yeske[42] to measure *in situ* corrosion rates of carbon steel in kraft pulping liquors showed poor agreement between LPR and weight loss measurements; however, the ratio of β to z was found to be a function of the solution at a given temperature, where z is the number of electrons released in the dissolution reaction, and β is given as:

$$\beta = \frac{\beta_a \times \beta_c}{(\beta_a + \beta_c)}. \quad [5]$$

Equation [5] is based on the theory of Stern and Geary.[43] Values for the Tafel slopes at different temperatures are therefore indicative of the effectiveness of sulfide oxidation more than metal dissolution.

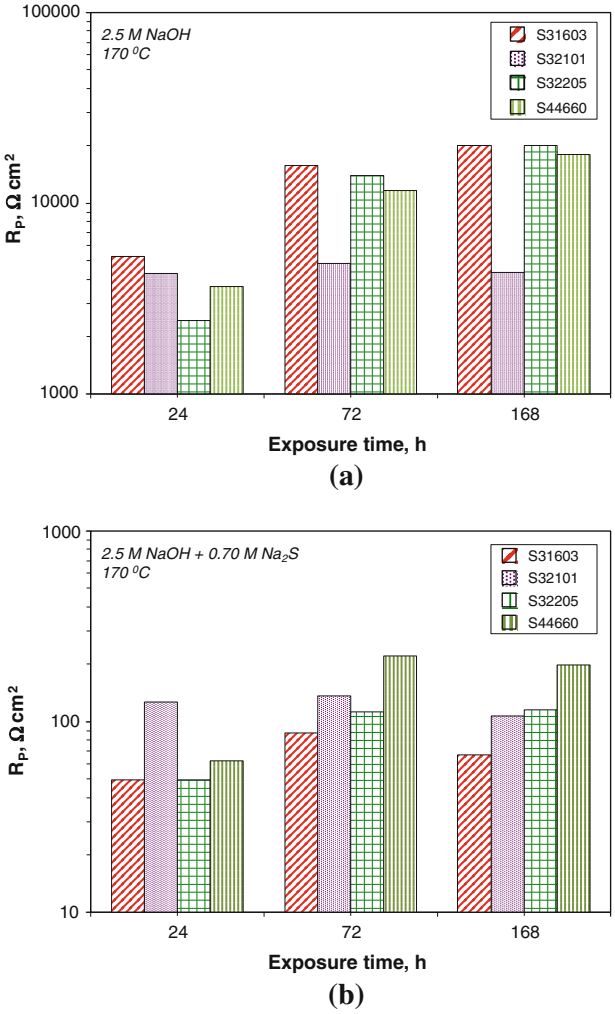

Fig. 5—Linear polarization resistance values during 168 h exposure of SFSS UNS S44660, austenitic UNS S31603, lean DSS UNS S32101, and standard DSS S32205 tested in (*a*) 2.5 M NaOH and (*b*) 2.5 M NaOH + 0.70 M Na_2S at 443 K (170 °C).

LPR measurements are indicative of differences in the efficiency of sulfide oxidation/reduction on the stainless steels with exposure to the 2.5 M NaOH + 0.70 M Na_2S solution.[42] Results from the LPR measurements shown in Figure 5(b) indicate that sulfide oxidation/reduction was least efficient on the SFSS UNS S44660 and most efficient on austenitic UNS S31603 based on the polarization resistance values. Drastic difference can be observed in the polarization resistance values between the simple NaOH solution (2 to 5 kΩ cm^2) and the solution with sulfide (70 to 200 Ω cm^2) after a 24 hours exposure, a reduction of nearly two orders of magnitude. There was no appreciable increase in the polarization resistance with exposure time for the stainless steel samples in the sulfide-containing solution after 72 hours of exposure. Results from the LPR measurements in the current study are consistent with findings from Ramo *et al.*[19,20] who showed that the adhesion of sulfur onto steel increased in the order UNS S32304, S32205, S30400, and S31603, correlating to the Cr content of the steel. Current results showed that the SFSS UNS S44660, having the highest Cr content, had the highest polarization resistance and austenitic UNS S31603, having the lowest Cr content, had the lowest polarization resistance. Measurements from the LPR technique generally correlated with the corrosion rates measured from the weight loss and potentiodynamic techniques in the current study.

D. *Surface Oxide Film Morphology and Composition*

The weight loss coupons were cleaned and examined after exposure to the caustic test solutions to observe the form of corrosion and surface morphology. General corrosion was observed in the SFSS UNS S44660 as well as the other stainless alloys in the simple NaOH solution. Cross-sectional SEM micrographs of the surface film that formed on lean DSS S32101 and standard DSS S32205 in 2.5 M NaOH at 443 K (170 °C) (Figure 6) show that visually there were two distinct regions of the oxide. EDS measurements taken from the two regions of the surface film were normalized for qualitative comparisons. The contributions of C and Al have been neglected. Results in Table III show that the outer layer of the lean and standard DSS was enriched in Fe and the inner layer was enriched in Cr and Ni. The outer layer surface compositions of S32101 and UNS S32205 were similar, but the inner layer compositions differed with respect to the concentrations of Ni, Mn, and Mo, owing to the differences in the nominal composition of the alloys. Ni was enriched in both lean DSS UNS S32101 and standard DSS S32205. Mn and Mo were detected in the inner surface film of the lean DSS UNS S32101 and standard DSS UNS S32205, respectively, in concentrations that were similar to the respective nominal compositions of the alloys. Na, Ca, and Si were detected in the films in less than 1 wt pct. It should be noted that the O contribution has an appreciable contribution to the measured values, and the ability of EDS to measure O can be limited.

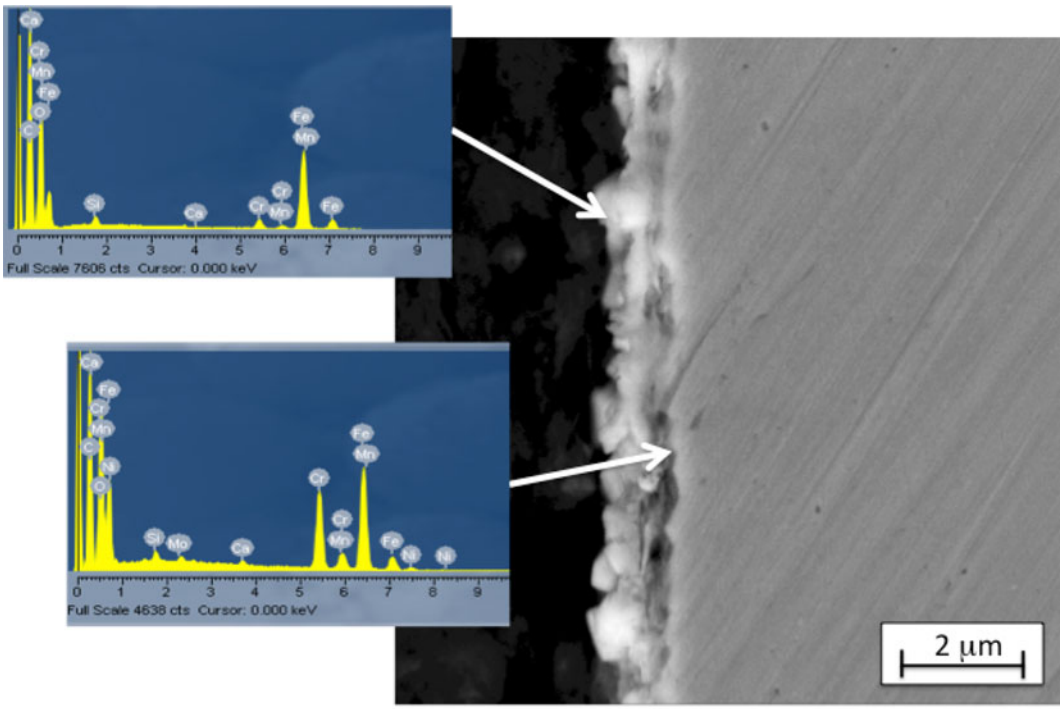

(a)

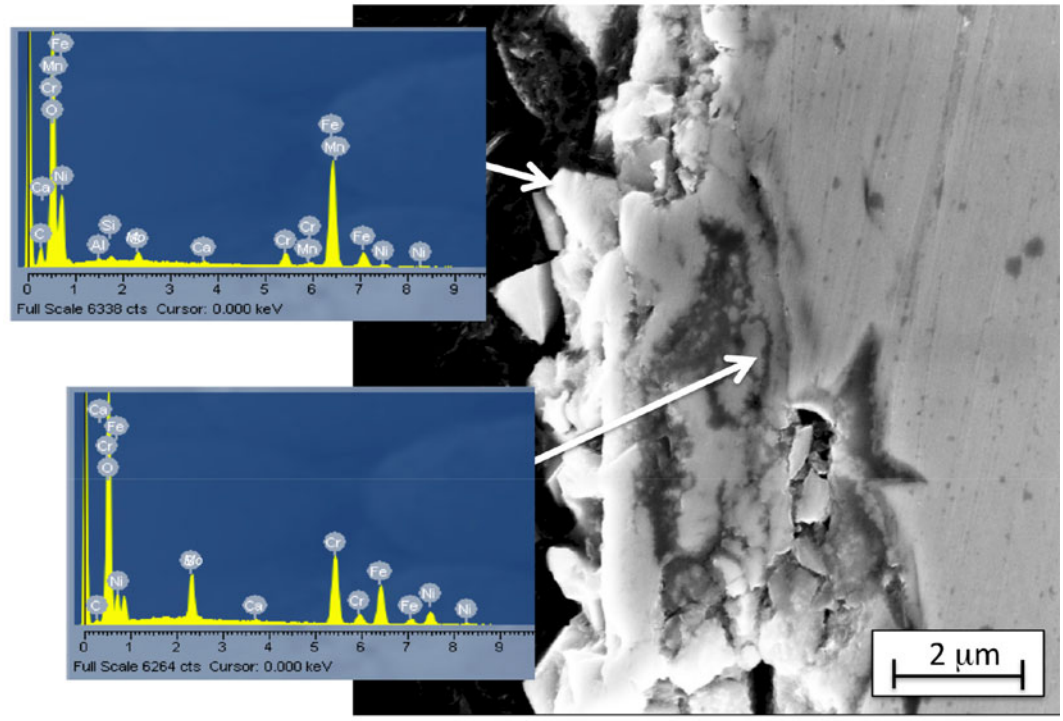

(b)

Fig. 6—Cross-sectional SEM micrographs showing the surface film that formed on (*a*) lean DSS UNS S32101 and (*b*) standard DSS UNS S32205 tested at the OCP for 168 h in 2.5 M NaOH at 443 K (170 °C). EDS spectra were measured at the regions identified by arrows.

Therefore, the results in Table III are semi-quantitative and demonstrate the differences among the film compositions.

The corrosion morphology on each of the stainless steel alloys was influenced by the presence of sulfide in the caustic solutions as shown in Figure 7. The SFSS UNS S44660 (Figure 7(a)) underwent intergranular corrosion. The SFSS did not have any obvious precipitates near the grain boundaries when polished and observed with the backscatter electron detector in the SEM or when etched to reveal the microstructure. Ti and Cb are intentionally added to SFSS to stabilize the

Table III. Normalized EDS Film Compositions (Weight Percent) Measured on Lean DSS UNS S32101 and Standard DSS UNS S32205 After a 168 h Exposure at the OCP in 2.5 M NaOH at 443 K (170 °C)

Alloy UNS Number	Film	O	Fe	Cr	Ni	Mo	Mn	Other*
S32101	outer	34	60	4	<1	<1	1	<1
S32101	inner	21	51	23	<1	1	3	<1
S32205	outer	30	63	3	2	1	1	<1
S32205	inner	23	37	25	9	3	1	<1

*Na, Ca, and Si were detected in amounts less than 1 wt pct.

microstructure.[1–3] EDS measurements near the grain boundaries showed that there were elevated levels of S, Ti, and C, indicating that the intergranular attack was caused by the preferential corrosion of carbides. The austenitic UNS S31603 underwent general corrosion in the presence of sulfide (Figure 7(b)), but more of the microstructural features, *i.e.*, twins and grain boundaries, was observed as compared to the simple caustic solution. The lean DSS UNS S32101 (Figure 7(c)) and standard DSS UNS S32205 (Figure 7(d)) underwent selective corrosion of one of the phases. EDS results indicated that the phase with greater corrosion resistance had higher levels of Cr and Mo as compared to the nominal material composition, suggesting this phase was ferrite and the corroded phase was austenite.[5,6]

The surface film that formed on SFSS UNS S44660 as well as the other stainless steel in 2.5 M NaOH + 0.70 M Na_2S solution at 443 K (170 °C) can be seen in the cross-sectioned samples in Figure 8. The films that formed in the presence of sulfide were generally defective and thicker than those in the simple caustic solution. Even the SFSS with higher Cr had regions where the film was defective and non-uniform. Selective corrosion of standard DSS UNS S32205 was apparent after exposure as shown in Figure 9, having a penetration depth of nearly 50 μm. EDS spectra measured in the oxidized region of the material suggested that the phase with higher Cr content was more resistant to oxidation. Therefore, selective corrosion of austenite had occurred, which resulted in oxidized austenite islands in the ferrite matrix. The normalized compositions determined by EDS shown in Table IV for all of the stainless steels indicated that the outer layers were enriched in S and Ni. Sulfidation of the oxide film occurred in all of the alloys that were tested. The inner layers were enriched in Cr due to the selective dissolution of Fe, Mo, and Mn. Ni was also enriched in the inner layer of austenitic UNS S31603 and standard DSS UNS S32205. Na, Ca, and Si were detected in amounts than 1 wt pct.

E. *X-ray Photoelectron Spectroscopic Measurements*

In order to evaluate selective dissolution of the main alloying elements in the stainless steels, *i.e.*, Cr, Ni, Mo, and Mn, in the simple NaOH solution, the surface oxide films formed at the OCP were examined using XPS with depth profiling. The surface film composition for the SFSS UNS S44660 was similar to the other alloys in the 2.5 M NaOH solution with the main constituents being: OH^-, O^{2-}, Fe^{2+}, Fe^{3+}, Cr^{3+}, Ni^{2+}. The outer layers of the film consisted primarily of Fe hydroxides and oxides, whereas the inner layers were a mixed oxide of primarily Fe and Cr. Curve fitting of the high-resolution spectra of the Fe species indicated that the binding energies (BE) of the Fe^{2+} (at 706.8 eV) and Fe^{3+} (at 710.8 eV) species corresponded to either Fe_3O_4 or a mixture of FeO and Fe_2O_3. The primary Cr oxidation state (Cr^{3+}) typically detected near 576.5 eV was attributed to Cr oxide, which is in good agreement with the literature.[22] Indeed, the film consisted of both oxides and hydroxides, but fitting of the O 1s spectra indicated that the hydroxide species (at 531.1 eV) were predominantly in the outermost layers of the film. The lean and standard DSSs had similar film compositions after exposure to the simple NaOH solution, indicating that the film composition was not appreciably influenced by the alloying differences in Mn or Mo concentration. A comparison of the major constituents of the surface film between XPS sputter depth profiles acquired from lean DSS UNS S32101 (4 to wt pct Mn) and standard DSS UNS S32205 (3.0 to 3.5 wt pct Mo) are shown in Figure 10. The primary y-axis shows the normalized cation concentration (at. pct), and the secondary y-axis shows the measured (abs.) anion concentration (at. pct). Based on thermodynamic predictions[39,40] for the temperature, pH, and electrochemical conditions in this study, the film would likely contain spinel oxides of Fe and Cr. Mn and Mo were mostly selectively dissolved from the surface films of the lean and standard DSS, respectively, which supports electrochemical studies of DSSs and their alloying elements (Fe, Cr, Ni, Mo, and Mn) in NaOH solution.[9] The surface films that form on stainless steels in many environments[22] have been shown to have two primary layers: an outer hydroxide layer and inner oxide layer. The XPS results from this study also support a bi-layer film in the simple NaOH environment.

The effect of sulfide on the surface oxide film of SFSS UNS S44660 compared to standard DSS UNS S32205 after exposure to the 2.5 M NaOH + 0.70 M Na_2S solution can be seen in Figure 11. The primary film constituents were: S^{2-}, OH^-, O^{2-}, Fe^{2+}, Fe^{3+}, Cr^{3+}, Ni^{2+}. The composition of the film varied considerably from the simple NaOH solution. The spectra corresponding to half of the maximum of the O 1s signal indicated that there was an appreciable amount of metal oxidation in the presence of sulfide as compared to the simple NaOH solution. Moreover, a broad shoulder was also associated with the high-resolution Ni 2p and Fe 2p spectra, which was not apparent in the NaOH solution. High-resolution XPS scans of Fe 2p, Cr 2p, Ni 2p, S 2p, and O 1s from the top surface layers formed on the

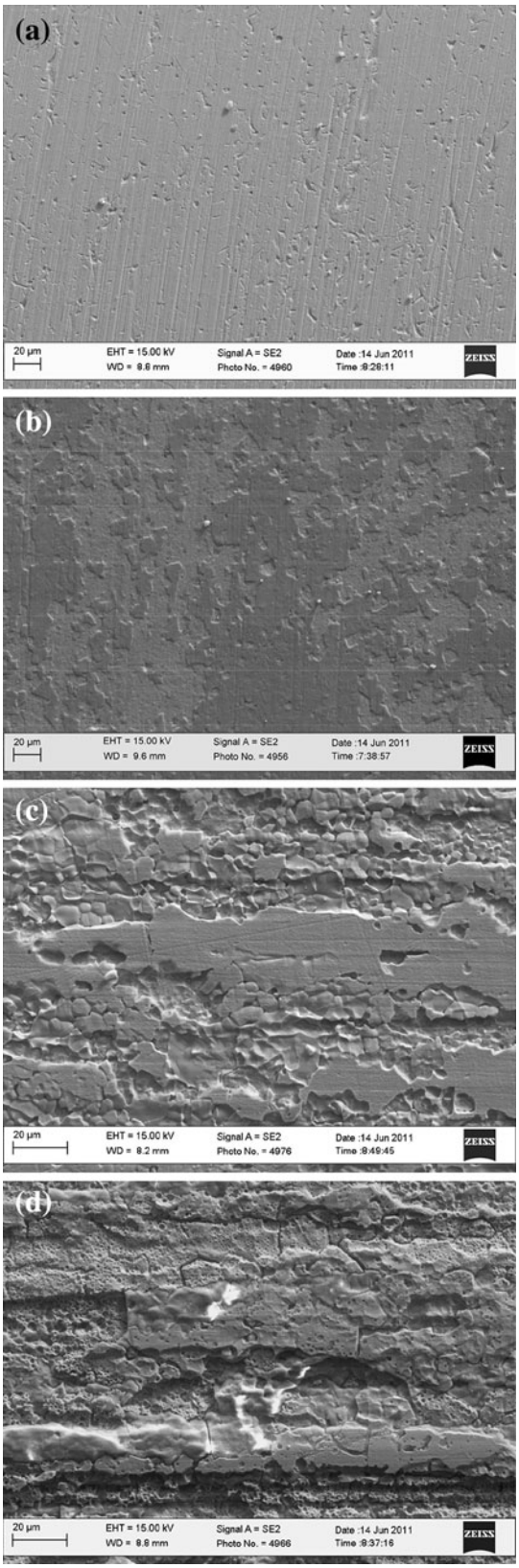

Fig. 7—SEM micrographs showing the cleaned surface of (*a*) SFSS UNS S44660, (*b*) austentic UNS S31603, (*c*) lean DSS UNS S32101, and (*d*) standard DSS UNS S32205 tested at the OCP for 168 h in 2.5 M NaOH + 0.70 M Na_2S at 443 K (170 °C).

stainless steels indicated that there were metal sulfides and hydroxides near the surface. The BE of the O 1s signal on the outer levels was consistent with a hydroxide layer. Sulfur species were detected in the outermost layers of the film, which implies that sulfides were adsorbed in the oxide. The outer layers were enriched in Cr^{3+} and Ni^{2+}. Based on the BE of Cr^{3+} (~576.4 eV) detected in the outer layers, the Cr was present mostly as an oxide and/or hydroxide. The Ni 2p spectra were fit to a peak near 852.6 eV, which based on the literature[30–34] corresponds to either metallic Ni or Ni sulfide. Ni-enrichment was also apparent near the oxide/metal interface, but the limited amount of sulfur detected at the interface suggested that this was primarily metallic Ni. Furthermore, Cr-enrichment near the oxide/metal interface indicates that the film was mainly Cr oxide and hydroxide compounds. Results for standard DSS UNS S32205 in Figure 11(b) also indicate the surface film formed at 443 K (170 °C) was also Cr- and Ni-enriched, particularly in the outer layers. Sulfur species were also detected in the surface oxide. Ni-enrichment of the outer surface layer of the standard DSS UNS S32205 as well as austenitic UNS S31603 indicates that Ni reacted to form metal sulfide compounds in these alloys. Mo was mostly dissolved from the outer layers of standard DSS UNS S32205 and austenitic UNS S31603, which was consistent with the results from simple NaOH solution. The surface film on lean DSS UNS S32101 was nonadherent in the test solution, thus XPS analysis of the film provided limited information.

High-resolution XPS spectra for the S 2p species are shown as a function of depth for SFSS UNS S44660 in Figure 12. The peaks in the high-resolution spectra for the S 2p species in the other stainless alloys also corresponded to a BE in the range of 160 to 165 eV. An attempt was made to fit curves to the S 2p spectra to determine the sulfur compounds that formed at the OCP in the sulfide-containing caustic solution. The fitting was performed at a depth corresponding to the oxide/metal interface (half the maximum O 1s signal, *i.e.*, ~2 nm). The reduced sulfur was present in various forms of sulfide. Sulfur peaks corresponded to S^{2-} at 161.9 eV (Full Width Half Max (FWHM) = 1.3 eV), and S_n^{2-} at 163.4 eV (FWHM = 1.0 eV). The S 2p peaks for the S_2^{2-} and S_n^{2-} peaks were detected at 162.5 and 164.7 eV, respectively. The peaks had similar FWHM and BE values as those identified in the literature for SRB at room temperature.[30–34] The relative amount of monosulfide to polysulfide increased with sputtering depth and was approximately 2:1 at the oxide/metal interface. The relative ratio of Fe, Cr, or Ni metal compounds could not be determined from the XPS data, but based on the relative concentration after sputtering to the oxide/metal interface, sulfides of Fe and Ni were most likely predominant in the outer layers of the film. The results imply that sulfur binds to the metal surface and is integrated into the oxide film, preventing stable passivation.

The solubility products and standard free energies of formation for the sulfide compounds that could form

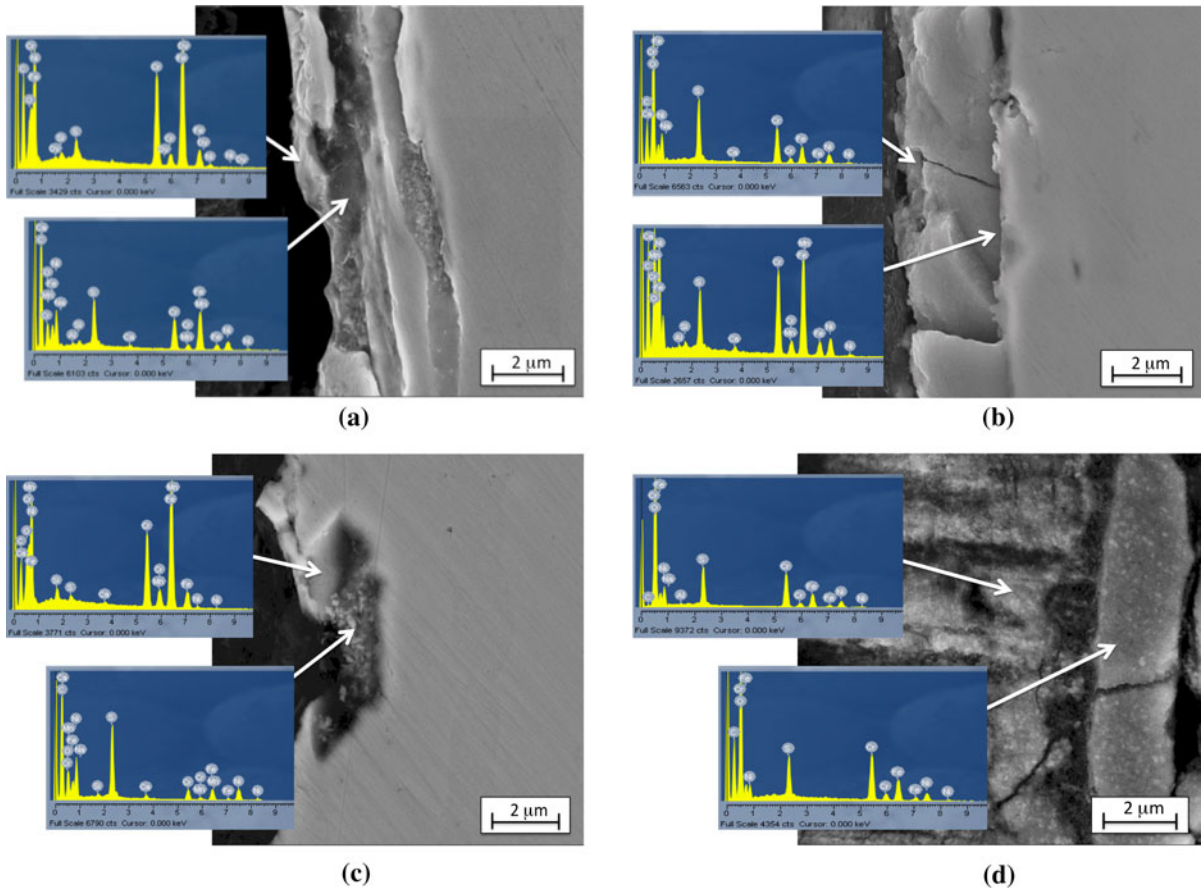

Fig. 8—Cross-sectional SEM micrographs showing the surface film that formed on (*a*) SFSS UNS S44660, (*b*) austentic UNS S31603, (*c*) lean DSS UNS S32101, and (*d*) standard DSS UNS S32205 tested at the OCP for 168 h in 2.5 M NaOH + 0.70 M Na_2S at 443 K (170 °C). EDS spectra were measured at the regions indicated by the arrows.

under the conditions in this study are compared in Table V. The Fe, Cr, and Ni sulfide compounds in this work were assumed to be stoichiometric. In reality, metal sulfide compounds are rarely stoichiometric due to the numerous oxidation numbers of sulfur.[40,41] In general, the more negative the free energy of formation ($\Delta G°$) and lower the solubility product (K_{sp}), the greater the likelihood the species is insoluble and would be detected in the oxide film after exposure to the test solution. The sulfide compounds have lower solubility products than the oxides. Limited solubility of the sulfide compounds is one explanation for the observed enrichment of sulfur on the outer surface layers in the EDS and XPS spectra.

Thermodynamic predictions (E-pH diagrams) were used to determine the stable species that can form near the OCP in the Fe-Cr-Ni-S–H_2O system at 443 K (170 °C). The E-pH diagrams for the dominant Fe, Cr, and Ni species are shown in Figure 13.[40] All molar concentrations are assumed to be 10^{-3} M for the metal cations and 0.70 M for sulfur. Cr did not form metal sulfide compounds in the E-pH region (ca. −1.10 V *vs* Ag/AgCl and pH 11.5) in this study based on the thermodynamic predictions. This finding was confirmed by the XPS measurements on the alloys. Based on the E-pH diagrams, FeS (ferric/ferrous sulfide) and Ni_3S_2 (heazlewoodite) were more likely to form under the conditions in this study. There are numerous FeS compounds reported in the literature. Mackinawite ($Fe_{1+x}S$) has been reported for pure iron[37] and carbon steel[38,39] previously. This form of iron sulfide is relatively unstable and difficult to characterize with XPS. Other forms of iron sulfide, *i.e.*, pyrrhotite ($Fe_{1-x}S$), troilite (FeS), pyrite (FeS_2), and greigite (Fe_3S_4), may also form. The BE value from DSS UNS S32205 was close to those reported for $Fe_{1+x}S$ in XPS studies of SRB, but it cannot be concluded if this form was present in the current study due to the complexity of the surface composition. Moreover, reported BE values for Ni_2S_3 are close to those for the FeS compounds, thus it cannot be determined what species was prevalent. Spectroscopy techniques, *i.e.*, XPS and EDS, have their inherent limitations such as quality of peak fitting and degradation during analysis. Nonetheless, the findings of this work support a corrosion mechanism of stainless steels in sulfide-containing caustic solution that is based on the adsorption of sulfide compounds that hinder the formation of a stable passive film.

All of the stainless steel samples exposed to caustic solution containing sodium sulfide at the OCP showed convincing evidence for the adsorption of sulfide species in the oxide film. Sulfide adsorption favored the

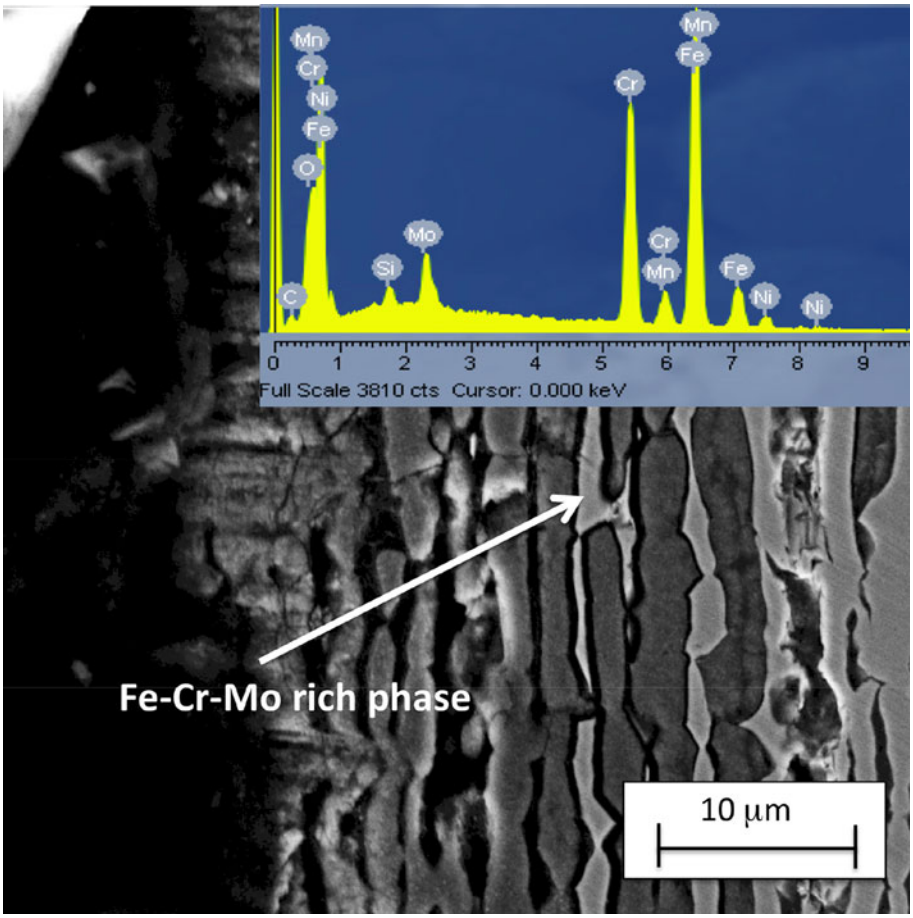

Fig. 9—Cross-sectional SEM micrograph showing the surface film that formed on standard DSS UNS S32205 tested at the OCP for 168 h in 2.5 M NaOH + 0.70 M Na_2S at 443 K (170 °C). EDS spectra were measured at the region indicated by the arrow.

Table IV. Normalized EDS Compositions (Weight Percent) Measured on SFSS UNS S44660, Austenitic UNS S31603, Lean DSS UNS S32101, and Standard DSS UNS S32205 After a 168 h Exposure at the OCP in 2.5 M NaOH + 0.70 M Na_2S at 443 K (170 °C)

Alloy UNS Number	Film	O	S	Fe	Cr	Ni	Mo	Mn	Other*
S44660	outer	9	6	51	23	9	<1	1	<1
S44660	inner	1	1	65	26	2	4	<1	<1
S31603	outer	21	11	20	26	9	<1	<1	<1
S31603	inner	10	3	53	20	2	<1	<1	<1
S32101	outer	38	8	38	8	6	<1	1	<1
S32101	inner	5	1	64	22	2	<1	4	<1
S32205	outer	27	12	16	25	20	<1	<1	<1
S32205	inner	31	9	18	27	14	<1	<1	<1

*Na, Ca, and Si were detected in amounts less than 1 wt pct.

formation of a defective film. Films were also defective because sulfide reacted with the steel to form non-protective metal sulfide compounds. Unlike the simple NaOH solution, Fe oxides and hydroxides were not detected in appreciable amounts on the outer layers of the surface film. The outer surface layer of the films that formed on the stainless steels in caustic solution containing sodium sulfide were composed largely of Cr oxide and hydroxide compounds as well as metal sulfides. Ni was present in the outer layers as a metal sulfide and in the inner layers in a metallic state. The outer layer of the surface film contained primarily Ni and Fe metal sulfide compounds, which is supported by thermodynamic predictions. Caustic solution, with or without sulfide, favored selective dissolution of Mo and Mn. The SFSS UNS S44660 was susceptible to sulfide adsorption in the oxide surface film in caustic solution; however, adsorption was limited to the outer few nanometers of the film because the higher Cr content of this alloy facilitated the formation of a more

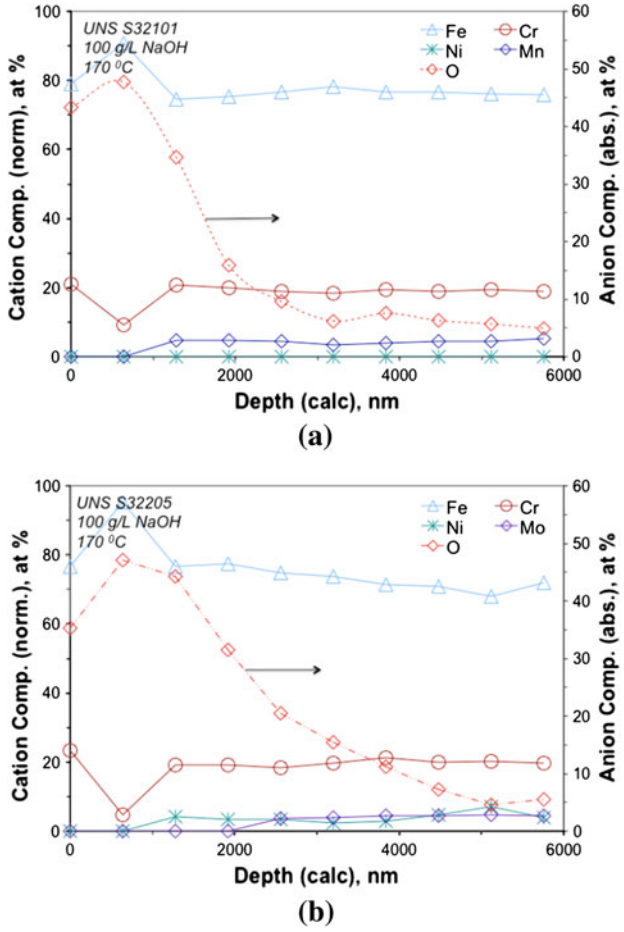

Fig. 10—XPS depth profile of the surface film on (*a*) lean DSS UNS S32101 and (*b*) standard DSS UNS S32205 after a 168 h exposure to 2.5 M NaOH at 443 K (170 °C).

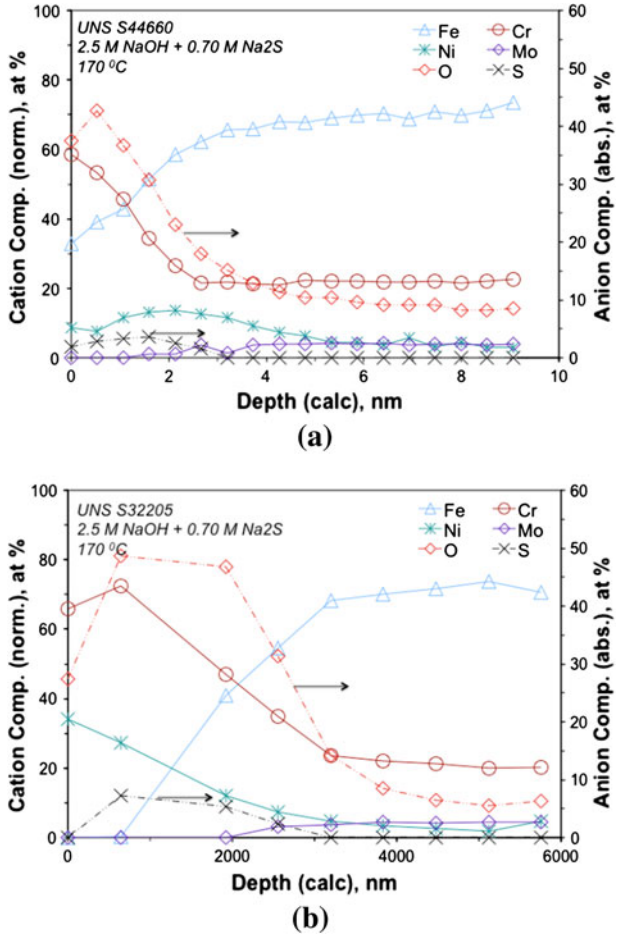

Fig. 11—XPS depth profile of the surface film on (*a*) SFSS UNS S44660 and (*b*) standard DSS (UNS S32205) after a 168 h exposure to 2.5 M NaOH + 0.70 M Na_2S at 443 K (170 °C).

protective oxide film as compared to the other stainless steels.

IV. SUMMARY

The effect of sodium sulfide on the corrosion mechanism of SFSS UNS S44660 was compared to several different commercial grades of stainless steel (UNS S31603, S32101, and S32205) in caustic solution containing sodium sulfide to simulate white liquor. The following conclusions are drawn from the results:

1. Corrosion rates in caustic solution containing sodium sulfide at 443 K (170 °C) were highest for UNS S31603 and lowest for UNS S44660 on the basis of weight loss and electrochemical measurements. Corrosion rates for UNS S32101 and UNS S32205 were slightly lower than that of UNS S31603 and appreciably higher than UNS S44660. Selective corrosion of the austenitic phase was observed in UNS S32205 and S32101 tested in caustic

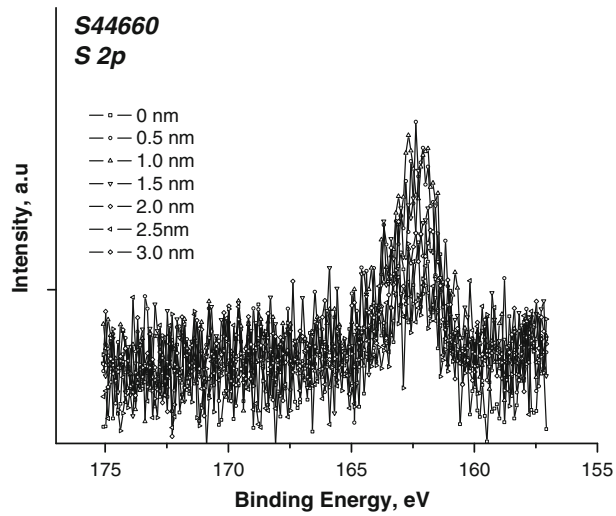

Fig. 12—High-resolution XPS spectra for S 2p species detected at different depths in the surface oxide layer of SFSS UNS S44660 after a 168 h exposure to 2.5 M NaOH + 0.70 M Na_2S at 443 K (170 °C).

Table V. Solubility Products for the Dominant Species the Fe-Cr-Ni Ternary System at 443 K (170 °C)

Element	Species	−Log K_{sp}	$\Delta G°$ [kcal mol^{-1}]
Fe			
	FeO	14.81	−56.3
	Fe_3O_4	26.75	−230.9
	Fe_2O_3	20.04	−167.7
	$HFeO_2^-$	28.47	−80.4
	FeS (II)	−15.55	−24.5
	FeS (III)	−66.66	−135.2
Cr			
	Cr_2FeO_4	0.70	−312.3
	CrO_4^{2-}	−41.55	−153.7
	$Cr(OH)_4^-$	−35.46	−227.3
	Cr_2S_3 (III)	−42.42	−86.0
Ni			
	Ni_3S_2 (II)	−52.52	−49.4
	NiO	6.68	−47.3

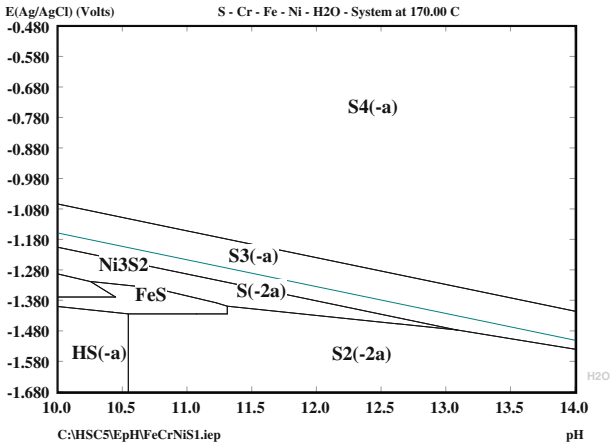

Fig. 13—E-pH diagram for the Fe-Cr-Ni-S–H_2O system (S dominant) at 443 K (170 °C) and 0.77 MPa. Molar concentration for metal is 0.001 M and sulfur is 0.70 M.[40]

solution containing sodium sulfide, but not in the simple caustic solution.

2. Potentiodynamic measurements indicated that sulfide significantly changed the anodic current density and Tafel slopes due to sulfide oxidation/reduction in caustic solution. The corresponding LPR results verified that the polarization resistance of UNS S44660 was greater than the other steels.
3. The surface oxide films that formed near the OCP on UNS S44660, UNS S31603, UNS S32101, and UNS S32205 became more defective after exposure to caustic solution containing sodium sulfide at 443 K (170 °C) owing to the adsorption of sulfide. The EDS and XPS spectra indicated that selective dissolution of Mo and Mn occurred in caustic solution, with and without sulfide, for the stainless steels that were tested.
4. Corrosion product morphologies and compositions imply that sulfide destabilized the oxide films and led to the formation of metal sulfides in all of the stainless steels that were tested in this study, but UNS S44660 was the most resistant to effect of sulfide adsorption due to the benefit of a higher Cr content.

ACKNOWLEDGEMENTS

Financial support by TIP3 (State of Georgia) and the member companies of the Institute of Paper Science and Technology, Georgia Tech is gratefully acknowledged. Kevin Chasse would also like to thank IPST at Georgia Tech for the PSE graduate student fellowship. Plymouth Tube Company and Outokumpu graciously donated UNS S44660 and UNS S32205, respectively. Dr. Penti Kinnunen and Dr. Timo Saario of VTT Technical Research Centre of Finland are acknowledged for useful discussions on electrochemistry.

REFERENCES

1. T.J. Nichol, I.A. Franson, and G.E. Moller: in *CORROSION/81*, NACE, Houston, TX, 1981, Paper No. 117.
2. N.J.E. Dowling, H. Kim, J.-N. Kim, S.-K. Ahn, and Y.-D. Lee: *Corrosion*, 1999, vol. 55, pp. 743–52.
3. H. Richaud-Minier and P. Gerard: in *NACE Corros. 2009 Conf. Expo.,* Atlanta, GA, 2009, Paper No. 09378.
4. D.L. Singbeil and A. Garner: *Corrosion*, 1985, vol. 41, pp. 634–39.
5. A. Wensley: in *Proc. 9th Int. Symp. Corros. Pulp Paper Ind.*, Ottawa, ON, Canada, 1998, pp. 27–37.
6. A. Wensley, M. Moskal, and W. Wilton: in *NACE Corrosion 97*, Houston, TX, 1997, Paper No. 378.
7. G. Rondelli, B. Vicentini, and E. Sivieri: *Corros. Sci.*, 1997, vol. 39 (6), pp. 1037–49.
8. J.H. Zheng, W.F. Bogaerts, and M.J. Brabers: *Corrosion*, 1992, vol. 48, pp. 320–31.
9. A. Bhattacharya and P.M. Singh: *Corros. Sci.*, 2011, vol. 53 (1), pp. 71–81.
10. A. Bhattacharya and P.M. Singh: *J. Fail. Anal. Prev.*, 2007, vol. 7 (5), pp. 371–77.
11. A. Bhattacharyaa and P.M. Singh: *Metall. Mater. Trans. A*, 2009, vol. 40A, pp. 1388–99.
12. G. Rondelli, I.B. Vicentini, M.F. Brunella, and A. Cigada: *Mater. Corros.*, 1993, vol. 44 (2), pp. 57–61.
13. K.R. Chasse and P.M. Singh: *Corrosion*, 2011, vol. 67 (1), p. 015002-1.
14. K.R. Chasse and P.M. Singh: *Corros. Eng. Sci. Technol.*, 2012, vol. 47 (3), pp. 170–76.
15. M. Honda, Y. Kobayashi, and A. Tamada: *Corrosion*, 1992, vol. 48, pp. 822–29.
16. H. Leinonen, P. Pohjanne, K.R. Chasse, P.M. Singh, J. Romu, T. Saukkonen, and H. Hänninen: *NACE Corros. 2012 Conf. Expo.*, Salt Lake City, UT, 2012, Paper No. 1746.
17. H.T. Leinonen, P. Pohjanne, T. Saukkonen, T. Schildt, J. Romu, and H. Hanninen: *NACE Corros. 2011 Conf. Expo.,* Houston, TX, 2011, Paper No. 11160.
18. P.M. Singh, O. Ige, and J. Mahmood: *Corrosion*, 2003, vol. 10, pp. 843–50.
19. J. Ramo, M. Sillanpaa, A. Kujalao, O. Hyokyvirta, and S. Peltonen: *Mater. Corros.*, 2001, vol. 52, pp. 531–39.
20. J. Ramo, M. Sillanpaa, A. Kujalao, O. Hyokyvirta, and S. Peltonen: *Mater. Corros.*, 2001, vol. 52, pp. 741–47.
21. I. Betova, M. Bojinov, O. Hyokyvirta, and T. Saario: *Corros. Sci.*, 2010, vol. 52, pp. 1499–507.
22. C.-O.A. Olsson and D. Landolt: *Electrochim. Acta*, 2003, vol. 48, pp. 1093–104.
23. C.L. McBee and J. Kruger: *Electrochim. Acta*, 1972, vol. 17, pp. 1337–41.

24. C. Pallotta, N. De Cristofaro, R.C. Salvarezza, and A.J. Arvia: *Electrochim. Acta*, 1986, vol. 31, pp. 1265–70.
25. E.J. Calvo and C.D. Pallotta: *J. Electroanal. Chem.*, 1986, vol. 198, pp. 181–86.
26. J.H. Gerretsen, J.H.W. de Wit, and J.C. Riviere: *Corros. Sci.*, 1990, vol. 31, pp. 545–50.
27. R. Kirchheim, B. Heine, S. Hofmann, and E.B. Yeager: *Corros. Sci.*, 1989, vol. 29, pp. 899–917.
28. S.C. Tjong, R.W. Hoffman, and E.B. Yeager: *J. Electrochem. Soc.*, 1982, vol. 129, pp. 1662–68.
29. Y. Jang, J. Son, S. Kim, and J. Lee: *Metall. Mater. Trans. A*, 2004, vol. 35A, pp. 3431–38.
30. C. Chen and C.R. Clayton: *J. Electrochem. Soc.*, 1997, vol. 144 (9), pp. 3140–46.
31. J. Duan, B. Hou, and Z. Yu: *Mater. Sci. Eng. C*, 2006, vol. 26, pp. 624–29.
32. P.J. Antony, R.K. Singh Raman, P. Kumar, and R. Raman: *Metall. Mater. Trans. A*, 2008, vol. 39A, pp. 2689–97.
33. C.R. Clayton, G.P. Halada, J.R. Kearns, J.B. Gillow, and A.J. Francis: in *Microbiologically Influenced Corrosion Testing*. J.R. Kearns and B.J. Little eds., ASTM STP 1232, Philadelphia, PA, 1994, pp. 141–152.
34. ASTM A268/A268M: *Standard Specification for Seamless and Welded Ferritic and Martensitic Stainless Steel Tubing for General Service*, ASTM International, West Conshocken, PA, 2010.
35. ASTM A240/A240M: *Standard Specification for Chromium and Chromium-Nickel Stainless Steel Plate, Sheet, and Strip for Pressure Vessels and for General Applications*, ASTM International, West Conshocken, PA, 2011.
36. Y. Yang, S. Kim, and J. Lee: *Metall. Mater. Trans. A*, 2005, vol. 36A, pp. 1229–36.
37. D.W. Shoesmith, M.G. Bailey, and B. Ikeda: *Electrochim. Acta*, 1978, vol. 23, pp. 1329–38.
38. D. Tromans: *J. Electrochem. Soc.*, 1980, vol. 127, pp. 1253–56.
39. R.C. Salvarezza, H.A. Videla, and A.J. Arvia: *Corros. Sci.*, 1982, vol. 22, pp. 815–29.
40. *HSC Chemistry 5.11*, Outokumpu Technology Engineering Research, Espoo, Finland, 2008.
41. M. Pourbaix: *Atlas of Electrochemical Equilibria in Aqeuous Solutions*, NACE, Houston, TX, 1974.
42. D.C. Crowe and R.A. Yeske: *IPC Technical Paper Series No. 191*, Institute of Paper Science, Atlanta, GA, 1986, 17 p.
43. M. Stern and A.L. Geary: *J. Electrochem. Soc.*, 1957, vol. 104 (1), pp. 56–63.